



# Simulation of early after-depolarisation in non-failing human ventricular myocytes: Can this help cardiac safety pharmacology?

Bernard Christophe

SCAP Test, rue d'Albroux, 10 – B-1367 Grand Rosière Hottomont, Belgium

**Correspondence:** Bernard Christophe, e-mail: bchristophe@scaptest.com

---

## Abstract:

**Background:** Identified as being the primary mechanism involved in the induction of torsades de pointes (TdP), early after-depolarisation (EAD) formation is an important parameter in cardiac safety pharmacology. Easily observed experimentally at the cellular or tissue level, EAD can also be simulated by computer algorithms using animal or human models. During the last decade, confidence in these algorithms has greatly increased. We investigated the putative usefulness of EAD simulation for cardiac safety pharmacology.

**Methods:** EAD simulations were performed in non-failing human ventricular myocytes using the O'Hara-Rudy dynamic model. The role of each cardiac current was investigated by modifying the amplitude of its activity in the model. Prediction of EAD induction by drugs was based on the ratio of their 50% inhibitory concentration values for various cardiac ionic currents to their maximal effective free therapeutic plasma concentration (EFTPC<sub>max</sub>).

**Results:** In the ventricular endocardial myocytes, EAD was only induced by at least 85% inhibition of the rapid delayed rectifier K<sup>+</sup> current (I<sub>Kr</sub>). The other currents can either induce or prevent EAD under sub- (80% I<sub>Kr</sub> inhibition) or up-threshold conditions (87% I<sub>Kr</sub> inhibition) of EAD. The study of the ability of drugs to induce EAD resulted in a classification which was in agreement with the Tdp risk classification.

**Conclusion:** Based on EAD computer simulation within the human situation, the present study identified the role of various cardiac currents in the EAD formation and suggested that prediction of EAD formation can be useful for early cardiac safety pharmacology.

## Key words:

early after-depolarisation, safety pharmacology, cardiac action potential simulation, ORd model, maximal effective free therapeutic plasma concentration

---

**Abbreviations:** AP – action potential, APA – maximal AP amplitude, APD<sub>xx</sub> – action potential duration at xx percent of the APA, CL – cycle length, EAD(s) – early after-depolarisation(s), EFTPC<sub>max</sub> – maximal effective free therapeutic plasma concentration, ORd model – O'Hara-Rudy dynamic model, RMP – resting membrane potential, TdP – torsades de pointes, T<sub>xx</sub> – triangulation at xx percent of APA, V<sub>max</sub> – maximal rate of AP rise

## Introduction

During the process of drug candidate discovery and/or development, reduction of the attrition rate is a major concern that remains to be solved by the pharmaceutical industry. Achieving this goal has strongly influ-

enced the fast emergence of scientific safety pharmacology in order to try to reveal cardiac liability earlier in this research process [3, 33, 38]. Among the various biomarkers that have been proposed for use in cardiac safety pharmacology, inhibition of the rapid delayed rectifying  $K^+$  channel current ( $I_{Kr}$ ) is crucial [34 for review]. This current controls the repolarisation of cardiomyocytes and a delay in this repolarisation leads to an abnormally long action potential (AP) often associated with an increased risk of cardiac arrhythmias. Nevertheless, various other cardiac ionic currents also influence this AP prolongation so that a multiple ion channel block is recognized as important for improving the early prediction of drugs' clinical torsadogenic risk [23]. The formation of early after-depolarisations (EADs) is also an important parameter in cardiac safety pharmacology as EADs are identified as being the primary mechanism involved in the induction of torsades de pointes (TdP) [2, 11, 15, 16]. EADs, defined as depolarisations occurring before the completion of AP repolarisation, are often associated with abnormally long AP observed with bradycardia or in the presence of a drug inducing prolongation of the action potential duration (APD) [5, 40, 41]. These EADs, generated in the presence of transmural heterogeneity during the ventricular repolarisation, can induce abnormal rhythmic cardiac activity resulting in severe cardiac arrhythmias such as TdP, polymorphic ventricular tachycardia or ventricular fibrillation. Easily observed experimentally at the cardiac cellular or tissue level of various species [4, 7, 12, 14, 16, 39], EAD induction has been demonstrated to be tissue- [17] and species-dependent [28]. On the other hand, EAD can also be simulated by computer algorithms using animal or human models. During the last decade, confidence in these algorithms has greatly increased [24]. Up to now, the recent O'Hara-Rudy dynamic (ORd) model based on isolated non-failing human ventricular myocytes [29] has been the only algorithm able to reproduce EAD within the human situation. Therefore, the present study using the ORd model is focused on EAD in order to determine the conditions and threshold of EAD formation in the human species and the factors inducing or suppressing EAD under sub- or up-threshold conditions of EAD. Finally, the opportunity to predict EAD induction by various drugs is studied and the putative role of EAD simulation in cardiac safety pharmacology is discussed.

## Materials and Methods

The ORd model equations used in the present study were fully described in O'Hara et al. [29] and in the research section of their website: <http://rudylab.wustl.edu>. Constants (extracellular ionic concentrations, cell geometry, channel conductance), initial conditions for state variables and scaling factors (applied to various ionic fluxes or to the conductance of various channels allowing differences among endo-, mid- and epimyocardial cells to be tested) were used as described in the ORd model. Simulations were carried out at equilibrium (after 100 beats) under a cycle length (CL) of 4000 ms in order to facilitate EAD formation. The impact of each current variation was calculated using the main equation of the model:

$$dv/dt = -(1 / Cm) \times (I_{tot} + I_{stim}) \quad (1)$$

where:  $dv$  = voltage membrane variation,  $dt$  = time variation,  $Cm$  = membrane capacitance,  $I_{tot}$  = sum of the various ionic currents and  $I_{stim}$  = stimulus current.

These various currents were  $I_{Na}$  (fast  $Na^+$  current),  $I_{NaL}$  (late  $Na^+$  current),  $I_{to}$  (transient outward  $K^+$  current),  $I_{CaL}$  ( $Ca^{++}$  current through the L-type  $Ca^{++}$  channel),  $I_{CaNa}$  ( $Na^+$  current through the L-type  $Ca^{++}$  channel),  $I_{CaK}$  ( $K^+$  current through the L-type  $Ca^{++}$  channel),  $I_{Kr}$  (rapid delayed rectifier  $K^+$  current),  $I_{Ks}$  (slow delayed rectifier  $K^+$  current),  $I_{K1}$  (inward rectifier  $K^+$  current),  $I_{NaCa_i}$  (myoplasmic component of  $Na^+/Ca^{++}$  exchange current),  $I_{NaCa_{ss}}$  (subspace component of  $Na^+/Ca^{++}$  exchange current),  $I_{NaK}$  ( $Na^+/K^+$  adenosine triphosphatase current),  $I_{Nab}$  ( $Na^+$  background current),  $I_{Kb}$  ( $K^+$  background current),  $I_{pCa}$  (sarcolemmal  $Ca^{++}$  pump current) and  $I_{Cab}$  ( $Ca^{++}$  background current).

The activity of all these various currents resulted in an AP linked to voltage membrane variations induced by a single electrical stimulation. This AP was described by using the following parameters: resting membrane potential (RMP) expressed as millivolts (mV), maximal amplitude of the AP (APA) expressed as mV, maximal rate of AP rise ( $V_{max}$ ) expressed as volts per second (V/s), duration of the AP measured at 40, 60 or 90% of APA inhibition ( $APD_{40, 60}$  or  $90$ ) expressed as milliseconds (ms) and finally AP triangulation estimations which were the difference between  $APD_{90}$  and  $APD_{40}$  or  $APD_{60}$  ( $T_{40}$  or  $60$ ) expressed as ms.

The shape of this AP can be modified by scaling either individually or simultaneously the conductance of these channels [6, 23]. Nevertheless, drugs influ-

ence the ionic current activity through various mechanisms such as channel conductance inhibition or activation, gate conformation changes, phosphorylation states, voltage sensitivity and/or expression level increase or decrease. In order to take into account all these various mechanisms, the change in a current activity was calculated by scaling up or down the activity of this current in the ORd model main equation (CL of 4000 ms) by multiplying the activity of the studied ionic current ( $I_{xx}$ ) by a scaling factor ( $SF_{xx}$ ). Depending on the amplitude of the induced effects (typical for each ionic current), the maximal values of this scaling factor could be ranked from 0.0 to 1.0-fold in the case of inhibition and from 1 to 30-fold in the case of activation of the ionic current. This scaling factor was applied either individually for a single ionic current or simultaneously for several ionic currents in the case of simulations regarding variations in single or multiple ionic currents, respectively.

In order to study the influence of a drug on the EAD formation within the human situation, a full profile of activity of this drug on all human cardiac ionic currents involved in the mechanism was required. Unfortunately, such a full profile has not been described in the literature for a large number of drugs, even though some databases are under construction such as Tox-database.net for example [32]. The data set published by Mirams et al. [23, Tab. 1] described 50% inhibitory concentration values ( $IC_{50}$ ) for  $I_{Na}$ ,  $I_{CaL}$  and  $I_{Kr}$  (determined by the whole cell patch clamp technique) and the maximal effective free therapeutic plasma concentration (EFTPC<sub>max</sub>) of 31 drugs. The great advantage of this data set was the well balanced distribution of these drugs within five classes with regard to their Tdp risk. Therefore, using the same data set allowed us to test the reliability of EAD formation simulation for early cardiac safety assessment. For each drug, the impact of  $I_{Na}$ ,  $I_{CaL}$  and  $I_{Kr}$  current activity changes was calculated in the ORd model main equation (CL of 4000 ms) by multiplying the activity of the three studied ionic currents ( $I_{Na}$ ,  $I_{CaL}$  and  $I_{Kr}$ ) by the following factors:

$$IC_{50_{xx}} / (EFTPC_{max} \times SF) \quad (2)$$

where  $IC_{50_{xx}}$  = 50% inhibitory concentration value for the studied ionic current ( $I_{Na}$ ,  $I_{CaL}$  or  $I_{Kr}$ ) and  $SF$  = the scaling factor (1, 3, 10, 30 or 100-fold) applied to EFTPC<sub>max</sub> (the highest value from Table 1 of Mirams et al. [23] was taken into account). These simultane-

ous changes in  $I_{Na}$ ,  $I_{CaL}$  and  $I_{Kr}$  currents activities allowed us to determine at which EFTPC<sub>max</sub> multiple each drug can potentially facilitate EAD formation.

## Results

### EAD formation

Using the ORd model under a CL of 4000 ms at equilibrium, stimulation of isolated non-failing human ventricular endocardial myocytes induced an AP characterized by the following parameters: RMP of -88.1 mV, APA of 129.9 mV,  $V_{max}$  of 280.3 V/s, APD<sub>40</sub> of 220.2 ms, APD<sub>60</sub> of 256.0 ms, APD<sub>90</sub> of 301.6 ms, T<sub>40</sub> of 81.4 ms and T<sub>60</sub> of 45.6 ms. Individual inhibition or activation of the various currents ( $I_{Na}$ ,  $I_{NaL}$ ,  $I_{Nab}$ ,  $I_{Kr}$ ,  $I_{Ks}$ ,  $I_{K1}$ ,  $I_{to}$ ,  $I_{Kb}$ ,  $I_{CaL}$ ,  $I_{CaNa}$ ,  $I_{CaK}$ ,  $I_{Cab}$ ,  $I_{NaCa}$ ,  $I_{NaCa}$ ,  $I_{NaK}$  or  $I_{pCa}$ ) differently modified the shape of this AP depending on the properties of each current. The  $I_{Na}$  current mainly (Fig. 1A) controlled both the AP and  $V_{max}$  amplitude (33.5% APA increase combined with 755.6%  $V_{max}$  increase induced by 30-fold  $I_{Na}$  activation vs. 5.5% APA decrease combined with 71.5%  $V_{max}$  decrease induced by 95%  $I_{Na}$  inhibition). In addition, 95%  $I_{Na}$  inhibition induced an abnormal AP delay (27.1% increase in the time required to reach APA and 29.6% APD<sub>90</sub> increase). An  $I_{Na}$  inhibition higher than 95% fully blocked AP formation. The  $I_{NaL}$  current mainly (Fig. 1B) controlled both the AP amplitude and duration. A 30-fold  $I_{NaL}$  activation induced a 23.9% APA increase combined with a huge AP rightward shift and triangulation (increase in APD<sub>40</sub>, APD<sub>60</sub>, APD<sub>90</sub>, T<sub>40</sub> and T<sub>60</sub> of 153.0, 162.1, 150.8, 145.2 and 87.8%, respectively). Conversely, full  $I_{NaL}$  inhibition induced only a slight decrease of APD<sub>40</sub>, APD<sub>60</sub> and APD<sub>90</sub> of 11.9, 11.8 and 10.8%, respectively. While  $I_{Nab}$  full inhibition (Fig. 1C) did not modify the AP shape,  $I_{Nab}$  activation induced only small AP variations. A 30-fold  $I_{Nab}$  activation induced RMP, APA and  $V_{max}$  decreases (6.7, 6.3 and 37.9%, respectively) combined with a small AP rightward shift and triangulation (increase in APD<sub>40</sub>, APD<sub>60</sub>, APD<sub>90</sub>, T<sub>40</sub> and T<sub>60</sub> of 14.6, 15.7, 24.2, 50.3 and 72.3%, respectively). The  $I_{Kr}$  current mainly (Fig. 2A) controlled the AP duration. An 84%  $I_{Kr}$  inhibition induced a huge AP rightward shift combined with a huge triangulation (increase in APD<sub>40</sub>, APD<sub>60</sub>, APD<sub>90</sub>, T<sub>40</sub> and T<sub>60</sub> of 99.4, 188.4, 183.8, 411.9 and

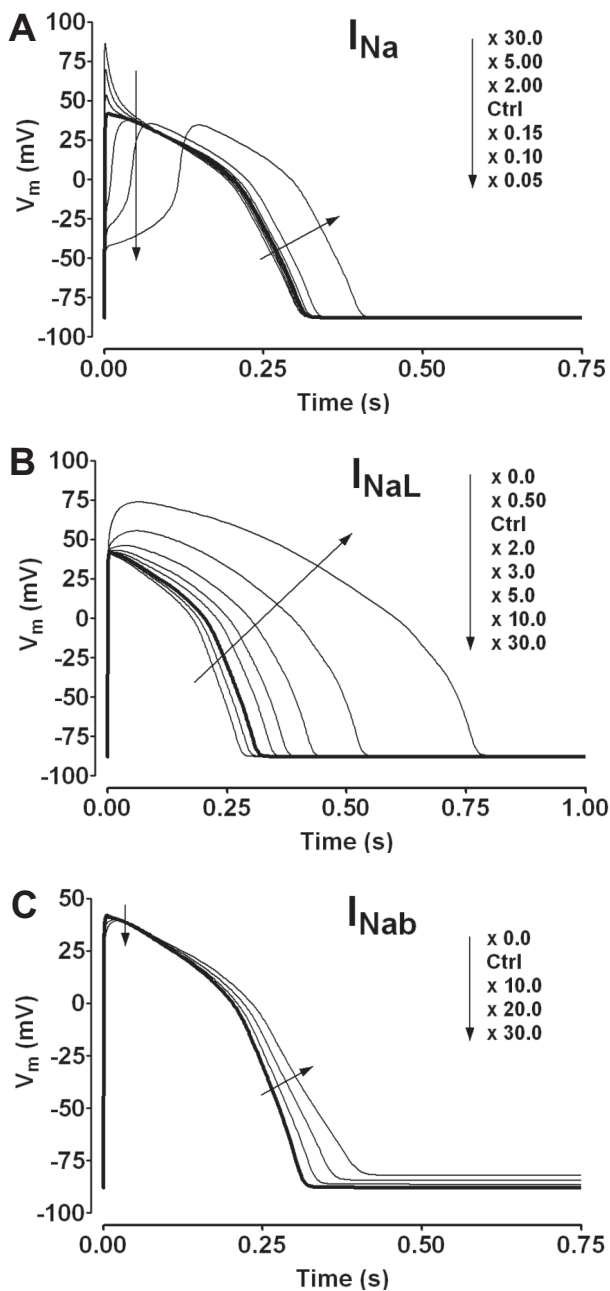


**Fig. 1.** Effects of  $I_{Na}$ ,  $I_{NaL}$  and  $I_{Nab}$  variations on the AP time course induced in non-failing human ventricular endocardial myocytes under a CL of 4000 ms at equilibrium. The bold line is the control AP (Ctrl). The scaling factor applied to the channel activity is indicated by arrows. The ordinate is the membrane voltage expressed as millivolts (mV). The abscissa is the time expressed as seconds (s)

157.8%, respectively). With 85%  $I_{Kr}$  inhibition, EAD (Fig. 2A) was observed at a take-off membrane potential of  $-22.2$  mV at 640.7 ms and a maximal membrane potential of 16.0 mV (APA at the EAD maximum of 103.8 mV) at 839.1 ms. A 30-fold  $I_{Kr}$  activa-

tion induced an AP leftward shift (decrease in  $APD_{40}$ ,  $APD_{60}$ ,  $APD_{90}$ ,  $T_{40}$  and  $T_{60}$  of 93.2, 93.0, 92.1, 89.1 and 86.8%, respectively). Like the  $I_{Kr}$  current, the  $I_{Ks}$  current mainly (Fig. 2B) controlled the AP duration. A 30-fold  $I_{Ks}$  activation induced an AP leftward shift (decrease in  $APD_{40}$ ,  $APD_{60}$ ,  $APD_{90}$ ,  $T_{40}$  and  $T_{60}$  of 41.2, 40.1, 36.9, 25.0 and 17.0%, respectively). Conversely, full  $I_{Ks}$  inhibition induced only a very small AP rightward shift without any triangulation (increase in  $APD_{40}$ ,  $APD_{60}$  and  $APD_{90}$  of 5.2, 5.3 and 4.5%, respectively). The  $I_{K1}$  current slightly (Fig. 2C) changed both the AP and  $V_{max}$  amplitude but mainly controlled the duration of the last repolarisation phase (14.6, 56.2 and 76.7% decrease with 15-fold  $I_{K1}$  activation vs. 15.0, 40.3 and 79.6% increase with full  $I_{K1}$  inhibition for  $APD_{90}$ ,  $T_{40}$  and  $T_{60}$ , respectively). An activation of  $I_{K1}$  higher than 15-fold blocked the AP formation. A full  $I_{to}$  inhibition (Fig. 2D) induced just a very slight APA increase (3.2%). Conversely, 30-fold  $I_{to}$  activation changed the AP shape by inducing an APA decrease and an AP rightward shift without any triangulation (8.7% APA decrease and 27.7, 25.5, 21.1% increase for  $APD_{40}$ ,  $APD_{60}$  and  $APD_{90}$ , respectively). The  $I_{Kb}$  current mainly (Fig. 2E) controlled the AP duration. A full  $I_{Kb}$  inhibition induced an AP rightward shift without any triangulation (17.9, 15.8 and 13.2% increase for  $APD_{40}$ ,  $APD_{60}$  or  $APD_{90}$ , respectively). On the other hand, a 30-fold  $I_{Kb}$  inhibition induced an APA decrease (7.9%) combined with  $APD_{40}$ ,  $APD_{60}$  and  $APD_{90}$  decreases (70.3, 45.2 and 26.3%, respectively) and a triangulation increase (92.7 and 82.1% for  $T_{40}$  and  $T_{60}$ , respectively). The  $I_{CaL}$  current (Fig. 3A) controlled both the AP amplitude and duration. While full  $I_{CaL}$  inhibition induced an AP leftward shift combined with triangulation (41.4, 29.6, 21.7, 34.4 and 22.8% for  $APD_{40}$ ,  $APD_{60}$ ,  $APD_{90}$ ,  $T_{40}$  and  $T_{60}$ , respectively), 30-fold  $I_{CaL}$  activation induced a very huge AP rightward shift combined with a huge triangulation (721.6, 853.4, 731.7, 759.1 and 48.7% for  $APD_{40}$ ,  $APD_{60}$ ,  $APD_{90}$ ,  $T_{40}$  and  $T_{60}$ , respectively). The  $I_{CaNa}$  current (Fig. 3B) also controlled both the AP amplitude and duration. While full  $I_{CaNa}$  inhibition did not change the AP parameters, 30-fold  $I_{CaNa}$  activation induced an APA increase (22.6%) combined with an AP rightward shift and triangulation (67.1, 67.2, 59.2, 37.9 and 14.0% for  $APD_{40}$ ,  $APD_{60}$ ,  $APD_{90}$ ,  $T_{40}$  and  $T_{60}$ , respectively). In the same way, the  $I_{CaK}$  current (Fig. 3C) controlled both the AP amplitude and duration. While full  $I_{CaK}$  inhibition did not change the AP parameters, 30-fold  $I_{CaK}$  activation induced an APA de-

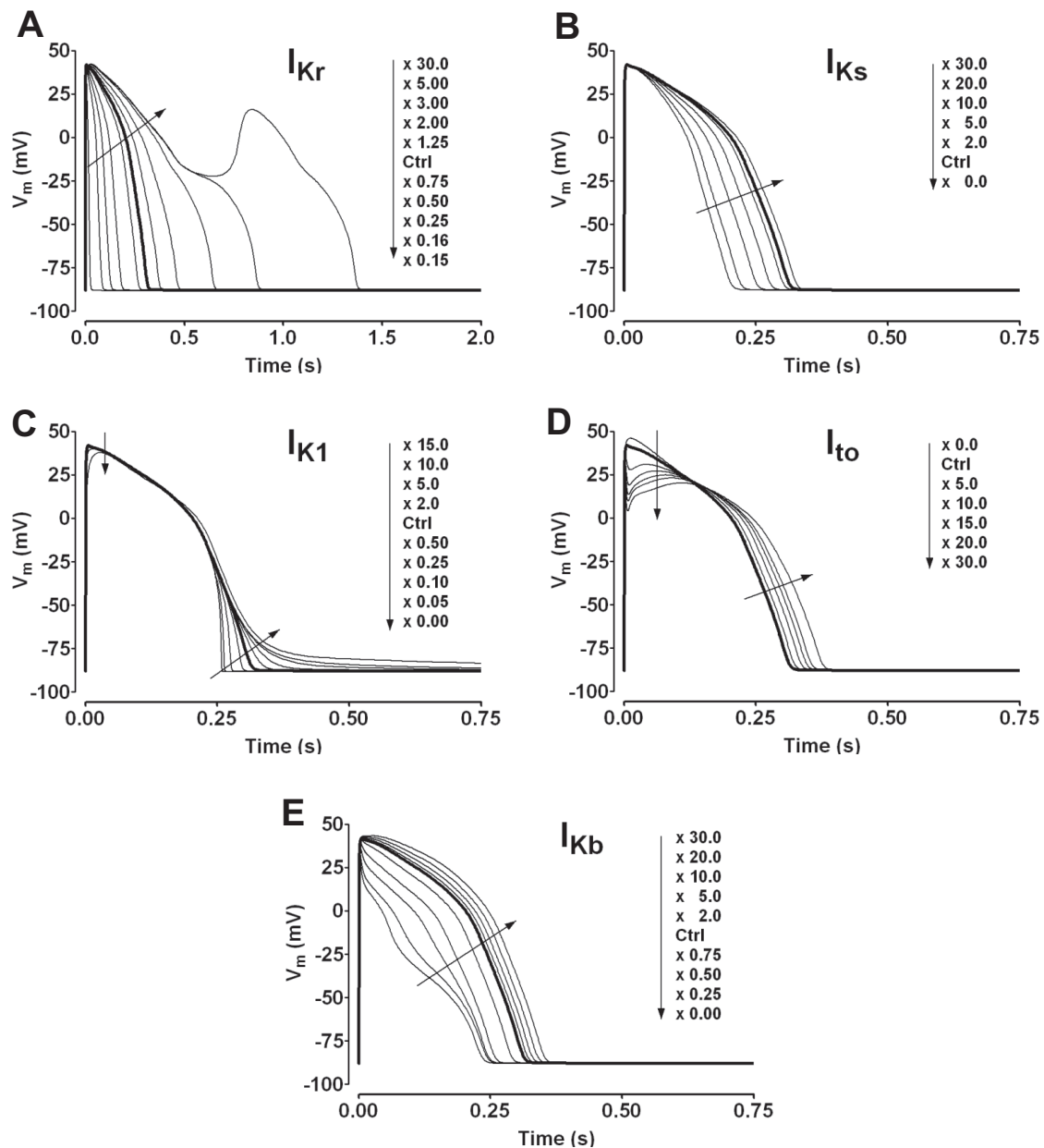


**Fig. 2.** Effects of  $I_{Kr}$ ,  $I_{Ks}$ ,  $I_{K1}$ ,  $I_{to}$  and  $I_{Kb}$  variations on the AP time course induced in non-failing human ventricular endocardial myocytes under a CL of 4000 ms at equilibrium. The bold line is the control AP (Ctrl). The scaling factor applied to the channel activity is indicated by arrows. The ordinate is the membrane voltage expressed as millivolts (mV). The abscissa is the time expressed as seconds (s)

crease (8.9%) combined with an AP rightward shift and triangulation (74.8, 116.4, 110.5, 206.9 and 77.1% for  $APD_{40}$ ,  $APD_{60}$ ,  $APD_{90}$ ,  $T_{40}$  and  $T_{60}$ , respectively). The  $I_{CaB}$  current (Fig. 3D) also controlled both the AP amplitude and duration. While full  $I_{CaK}$  inhibition did not change the AP parameters, 30-fold  $I_{CaK}$  activation induced a decrease of RMP (7.7%), APA (7.4%) and  $V_{max}$  (45.9%) combined with an AP rightward shift and triangulation (10.2, 10.5, 20.7, 48.8

and 77.9% for  $APD_{40}$ ,  $APD_{60}$ ,  $APD_{90}$ ,  $T_{40}$  and  $T_{60}$ , respectively). The  $I_{NaCa}$  current mainly (Fig. 4A) controlled both the activation speed and AP duration. While full  $I_{NaCa}$  inhibition did not change the AP parameters, 14-fold  $I_{NaCa}$  activation induced a  $V_{max}$  decrease (11.5%) combined with an AP rightward shift and triangulation (94.6, 132.0, 147.8, 291.4, 236.4% for  $APD_{40}$ ,  $APD_{60}$ ,  $APD_{90}$ ,  $T_{40}$  and  $T_{60}$ , respectively). An  $I_{NaCa}$  activation higher than 14-fold induced ab-

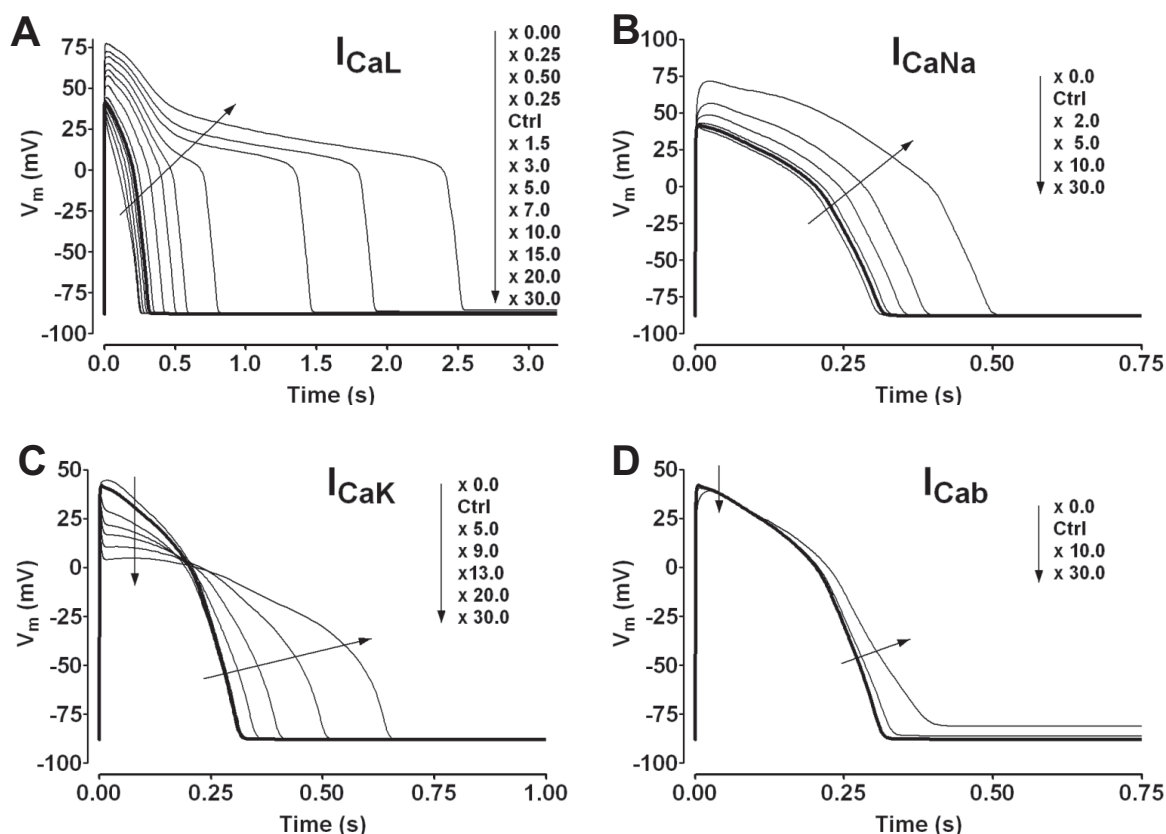


**Fig. 3.** Effects of  $I_{CaL}$ ,  $I_{CaNa}$ ,  $I_{CaK}$  and  $I_{Cab}$  variations on the AP time course induced in non-failing human ventricular endocardial myocytes under a CL of 4000 ms at equilibrium. The bold line is the control AP (Ctrl). The scaling factor applied to the channel activity is indicated by arrows. The ordinate is the membrane voltage expressed as millivolts (mV). The abscissa is the time expressed as seconds (s)

normal RMP and AP shape (data not shown). The  $I_{NaCass}$  current mainly (Fig. 4B) controlled both the AP amplitude and duration. While full  $I_{NaCass}$  inhibition did not change the AP parameters, 20-fold  $I_{NaCass}$  activation induced an APA increase (7.9%) combined with an AP rightward shift and triangulation (74.5, 88.2, 87.6, 123.0 and 84.5% for  $APD_{40}$ ,  $APD_{60}$ ,  $APD_{90}$ ,  $T_{40}$  and  $T_{60}$ , respectively). An  $I_{NaCass}$  activation higher than 20-fold induced abnormal RMP and AP shape (data not shown). The  $I_{NaK}$  current (Fig. 4C) controlled both the AP speed of activation and duration. Full  $I_{NaK}$  inhibition induced an AP slight rightward shift combined with a slight triangulation (8.3, 8.3, 7.7, 6.1 and 4.3% for  $APD_{40}$ ,  $APD_{60}$ ,  $APD_{90}$ ,  $T_{40}$  and  $T_{60}$ , respectively). Conversely, 30-fold  $I_{NaK}$  activation induced a RMP increase (11.0%) combined with a  $V_{max}$  decrease (55.0%) but also an AP leftward shift combined with a triangulation decrease (66.3, 65.1, 63.6, 56.4 and 55.7% for  $APD_{40}$ ,  $APD_{60}$ ,  $APD_{90}$ ,  $T_{40}$  and  $T_{60}$ , respectively). Finally, the  $I_{pCa}$  current (data not shown) did not change AP parameters.

In summary, the present simulations on the human endomyocardial cells under a CL of 4000 ms showed that AP prolongation (higher than 10%) was observed with the activation of nine different currents or the inhibition of three other currents. These various currents were ranked as follows:  $I_{Cab} \approx I_{Nab} \approx I_{to} < I_{CaNa} < I_{NaCass} < I_{CaK} < I_{NaCai} < I_{NaL} \ll I_{CaL}$  or  $I_{Kb} \approx I_{Na} \ll I_{Kr}$  with regard to the amplitude of APD prolongation induced after their activation or inhibition, respectively. An AP triangulation was always combined with this APD increase, except with  $I_{to}$  activation or  $I_{Kb}$  inhibition. In the same way, changes in APA and/or in  $V_{max}$  were always combined with this APD increase except with  $I_{Kr}$  inhibition. Indeed, under an 84%  $I_{Kr}$  inhibition, a huge APD increase combined with a huge triangulation was observed without any change in RMP, APA or  $V_{max}$ . Nevertheless, only  $I_{Kr}$  inhibition (at least 85%) was able to induce EAD in endomyocardial cells (see Fig. 5A). Increasing this percentage of inhibition induced a slight decrease of the EAD amplitude (APA from 103.8 to 79.3 mV for 85 to 95% inhibition,

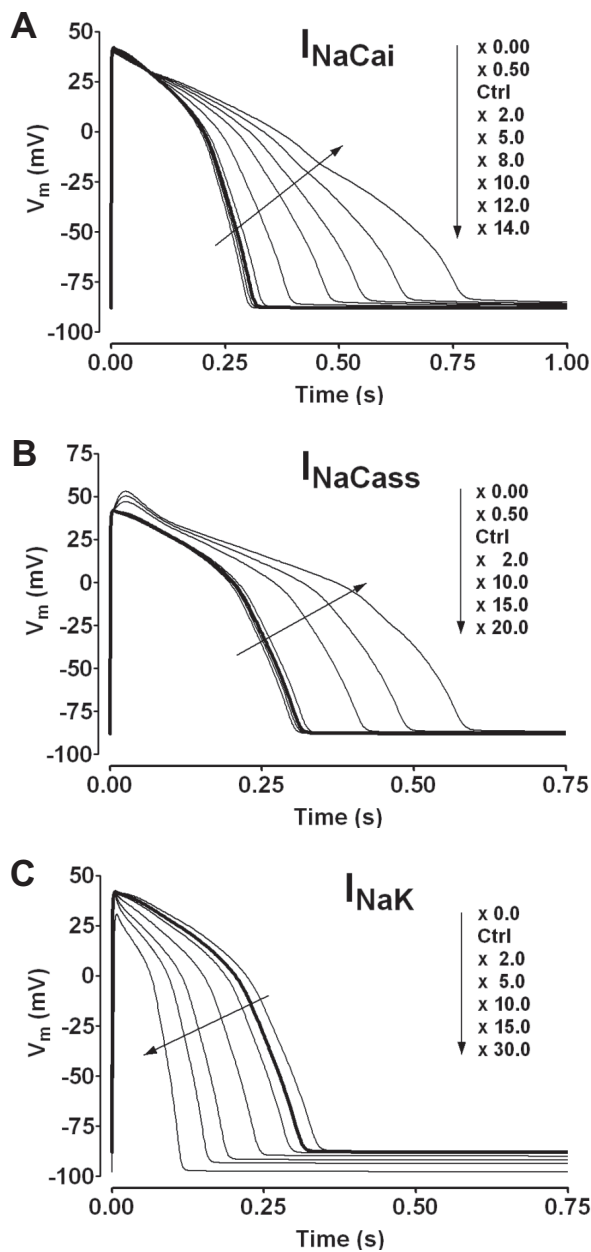


**Fig. 4.** Effects of  $I_{NaCai}$ ,  $I_{NaCass}$  and  $I_{NaK}$  variations on the AP time course induced in non-failing human ventricular endocardial myocytes under a CL of 4000 ms at equilibrium. The bold line is the control AP (Ctrl). The scaling factor applied to the channel activity is indicated by arrows. The ordinate is the membrane voltage expressed as millivolts (mV). The abscissa is the time expressed as seconds (s)

respectively), which was observed somewhat earlier (from 839.1 to 816.6 ms for 85 to 95% inhibition, respectively). Multiple EADs or sustained depolarisation were observed at 90 or 95%  $I_{Kr}$  inhibition, respectively. This high  $I_{Kr}$  inhibition (> 84%) induced EAD when the AP prolongation measured after 84%  $I_{Kr}$  inhibition was shorter than that measured after a 30-fold

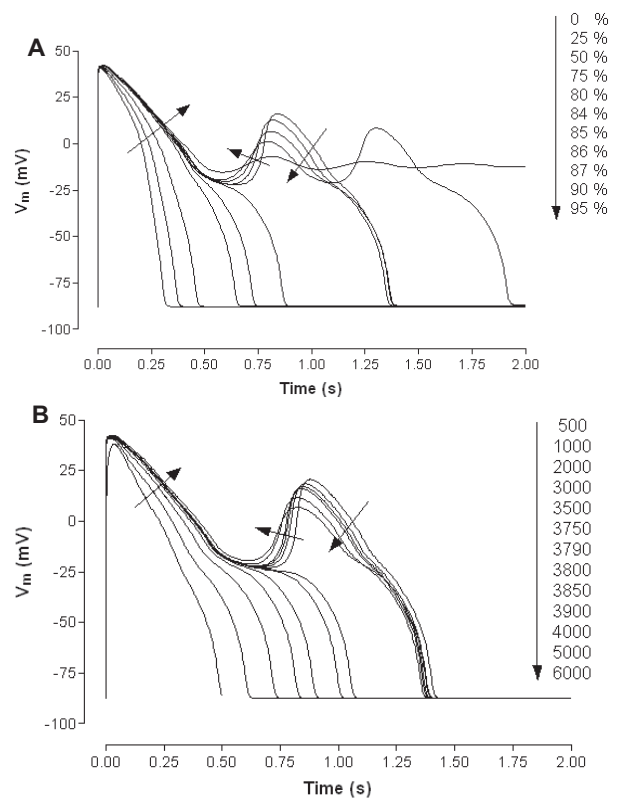


**Fig. 5.** (A) Effects of various percentages of inhibition of  $I_{Kr}$  on AP induced in non-failing human ventricular endocardial myocytes under a CL of 4000 ms at equilibrium. Changes in the percentage are indicated by arrows. The ordinate is the membrane voltage expressed as millivolts (mV). The abscissa is the time expressed as milliseconds (ms). (B) Effects of various CLs in the presence of 85%  $I_{Kr}$  inhibition on AP induced in non-failing human ventricular endocardial myocytes at equilibrium. Changes in the CL are indicated by arrows. The ordinate is the membrane voltage expressed as millivolts (mV). The abscissa is the time expressed as milliseconds (ms)

$I_{CaL}$  activation (13.8, 22.1 and 25.1-fold for  $APD_{40}$ ,  $APD_{60}$  and  $APD_{90}$ , respectively). The AP triangulation induced by 84%  $I_{Kr}$  inhibition showed a triangulation  $T_{40}$  54-fold smaller but a  $T_{60}$  3.2-fold higher than that induced by 30-fold  $I_{CaL}$  activation. Another major difference between  $I_{Kr}$  inhibition and  $I_{CaL}$  activation was the membrane voltage range in which the major part of the APD prolongation lingered (from 0 to -25 mV and from 25 and 0 mV for  $I_{Kr}$  inhibition and  $I_{CaL}$  activation, respectively).

In addition to the major role of ionic currents, bradycardia also controlled EAD formation. For example, under 85%  $I_{Kr}$  inhibition, endomyocardial cells (Fig. 5B) developed EAD only with a CL longer than 3790 ms. With a CL less than or equal to 3790 ms, a progressive increase in  $APD_{60}$  (from 376.8 ms to

912.9 ms for CL from 500 ms to 3790 ms, respectively) and APD<sub>90</sub> (from 476.7 ms to 1046.4 ms for CL from 500 ms to 3790 ms, respectively) was observed without any EAD induction. Conversely, EAD was induced with a CL ranked from 3800 to 6000 ms. The EAD amplitude slightly decreased (from 108.1 to 94.1 mV for CL from 3800 to 6000 ms, respectively) and was observed slightly earlier (from 877.1 to 822.4 ms for CL from 3800 to 6000 ms, respectively) depending on CL length.

In addition to the role of ionic currents and bradycardia, the cellular type also controlled EAD formation: midmyocardial cells were more sensitive to I<sub>Kr</sub> inhibition than endo- and epimyocardial cells. For example, with a CL of 1000 ms, EAD was observed on mid-, endo- and epimyocardial cells from 68, 95 or 100% I<sub>Kr</sub> inhibition, respectively. With a CL of 4000 ms, an I<sub>Kr</sub> inhibition of at least 62, 85 or 91% I<sub>Kr</sub> inhibition was required to EAD induction for mid-, endo- and epimyocardial cells, respectively.

#### EAD formation or suppression under sub- or up-threshold conditions of EAD

From the ORd model, an I<sub>Kr</sub> inhibition of 85% was the minimal level of inhibition required to EAD formation in isolated non-failing human ventricular endomyocytes under a CL of 4000 ms. Under a sub-threshold level of EAD (80% I<sub>Kr</sub> inhibition), the influence of inhibition or activation of various ionic currents on EAD formation can be studied. Conversely, under an up-threshold level of EAD (87% I<sub>Kr</sub> inhibition), the influence of inhibition or activation of various ionic currents on EAD suppression can be studied.

Even a full inhibition of I<sub>Na</sub>, I<sub>NaL</sub>, I<sub>to</sub>, I<sub>CaL</sub>, I<sub>CaNa</sub>, I<sub>CaK</sub>, I<sub>K1</sub>, I<sub>NaCai</sub>, I<sub>NaCass</sub>, I<sub>NaK</sub>, I<sub>Nab</sub>, I<sub>Kb</sub>, I<sub>pCa</sub> or I<sub>Cab</sub> combined with 80% I<sub>Kr</sub> inhibition did not facilitate EAD formation. On the other hand, a minimal 72% I<sub>Ks</sub> inhibition combined with 80% I<sub>Kr</sub> inhibition facilitated EAD formation. Even a huge activation (30-fold) of I<sub>Na</sub>, I<sub>to</sub>, I<sub>CaK</sub>, I<sub>Ks</sub>, I<sub>K1</sub>, I<sub>NaK</sub>, I<sub>Kb</sub> or I<sub>pCa</sub> combined with 80% I<sub>Kr</sub> inhibition did not facilitate EAD formation. On the other hand, activation of the other currents combined with 80% I<sub>Kr</sub> inhibition facilitated EAD formation: these effects were observed from an activation of 1.5, 1.9, 2.0, 6.0, 7.0, 8.0 and 8.0-fold for I<sub>CaL</sub>, I<sub>NaCai</sub>, I<sub>NaCass</sub>, I<sub>NaL</sub>, I<sub>Nab</sub>, I<sub>CaNa</sub> and I<sub>Cab</sub>, respectively.

Even a full inhibition of I<sub>to</sub>, I<sub>CaNa</sub>, I<sub>CaK</sub>, I<sub>Ks</sub>, I<sub>K1</sub>, I<sub>NaK</sub>, I<sub>Nab</sub>, I<sub>Kb</sub>, I<sub>pCa</sub> or I<sub>Cab</sub> combined with 87% I<sub>Kr</sub> inhibition did not induce EAD suppression. On the other hand,

inhibition of the other currents combined with 87% I<sub>Kr</sub> inhibition induced EAD suppression: these effects were observed from 15, 42, 43, 63 and 80% inhibition of I<sub>CaL</sub>, I<sub>NaCai</sub>, I<sub>NaCass</sub>, I<sub>Na</sub> and I<sub>NaL</sub>, respectively. Even a huge activation (up to 30-fold) of I<sub>Na</sub>, I<sub>NaL</sub>, I<sub>CaL</sub>, I<sub>CaNa</sub>, I<sub>NaCai</sub>, I<sub>NaCass</sub>, I<sub>Nab</sub>, I<sub>pCa</sub> or I<sub>Cab</sub> combined with 87% I<sub>Kr</sub> inhibition did not induce EAD suppression. On the other hand, activation of the other currents combined with 87% I<sub>Kr</sub> inhibition induced EAD suppression: these effects were observed from 1.3, 1.3, 2.1, 4.0, 7.0 and 20.0-fold for I<sub>Ks</sub>, I<sub>NaK</sub>, I<sub>K1</sub>, I<sub>Kb</sub>, I<sub>to</sub> and I<sub>CaK</sub>, respectively.

A similar global picture (data not shown) was obtained testing EAD formation or suppression under sub- or up-threshold levels of EAD with epi- or midmyocardial cells, notwithstanding the shift in sensitivity (lower for epimyocardial cells and higher with midmyocardial cells) already observed with these two types of cells.

#### Reference compounds and EAD formation

Various reference compounds were tested for their potency to facilitate EAD formation in the non-failing human endo-, mid- and epimyocardial cells (CL of 4000 ms) taking into account the ratio of their IC<sub>50</sub> for I<sub>CaL</sub>, I<sub>Na</sub> and I<sub>Kr</sub> to their EFTPC<sub>max</sub> (see Materials and Methods section). Depending on their risk of inducing Tdp, these 31 drugs were classified in five classes [34]: class I (class Ia and III anti-arrhythmics having a large but acceptable Tdp risk), class II (drug withdrawn from the market due to unacceptable Tdp risk), class III (drugs with numerous Tdp case reports), class IV (drugs with isolated Tdp case reports) and class V (drugs with no published Tdp case reports).

On the endomyocardial cells, no EAD (Fig. 6A) was induced with drugs from class V (cibenzoline, diltiazem, nitrendipine, phenytoin, propranolol, risperidone and verapamil) or class IV (amitriptyline, desimipramine, diphenylhydramine, fluvoxamine, imipramine, mexiletine, mibefradil, nifedipine, propafenone and quetiapine) even at 100-fold their EFTPC<sub>max</sub>. Drugs from class III either induced no EAD (bepridil, chlorpromazine or pimozone) even at 100-fold their EFTPC<sub>max</sub> or induced EAD (haloperidol or sertindole) only at 100-fold their EFTPC<sub>max</sub>. EAD was always observed with drugs from class II: prenylamine at 30-fold its EFTPC<sub>max</sub>, cisapride and terfenadine at 10-fold their EFTPC<sub>max</sub> and thioridazine at its EFTPC<sub>max</sub>. Regarding drugs from class I,

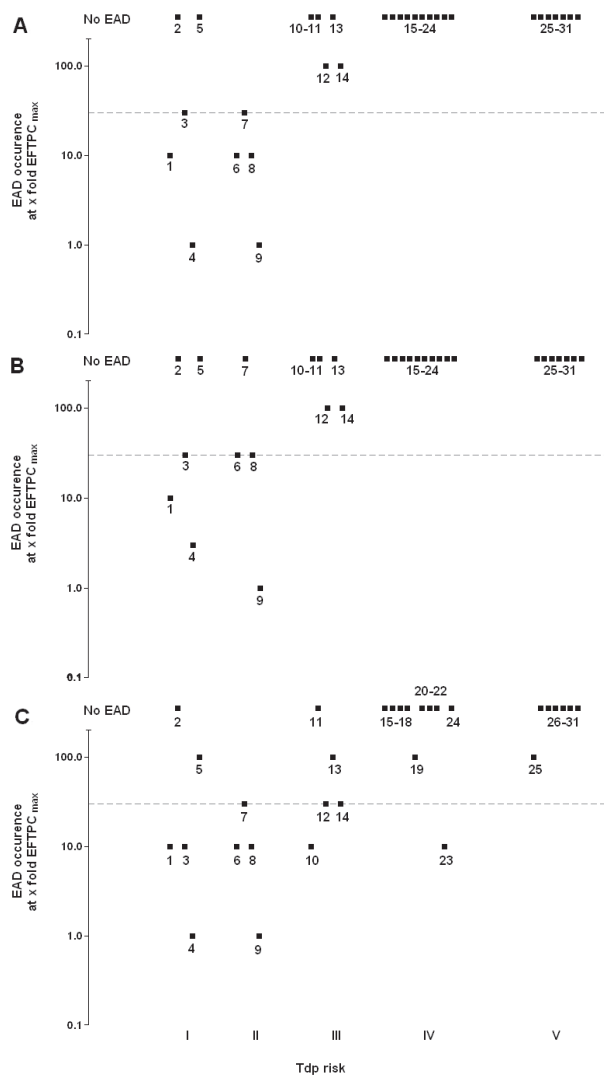


**Fig. 6.** Comparison of drugs ability to induce EAD calculated using the ORD model simulation (see Materials and Methods). EAD formation expressed as x-fold the EFTPC<sub>max</sub> observed in endo- (A), epi- (B) and midmyocardial (C) cells. The dotted line is the safety factor of 30. The risk of torsades de pointes (Tdp risk) is classified as follows [23, 34]: (I) Class Ia and III anti-arrhythmics having a large but acceptable Tdp risk, (II) drug withdrawn from the market due to unacceptable Tdp risk, (III) numerous Tdp case reports, (IV) isolated Tdp case reports and (V) no published Tdp case reports. Tested drugs are the following: ajmaline (1), amiodarone (2), dofetilide (3), quinidine (4), tedisamil (5), cisapride (6), prenylamine (7), terfenadine (8), thioridazine (9), bepridil (10), chlorpromazine (11), haloperidol (12), pimoziide (13), sertindole (14), amitriptyline (15), desimipramine (16), diphenylhydramine (17), fluvoxamine (18), imipramine (19), mexiletine (20), mibefradil (21), nifedipine (22), propafenone (23), quetiapine (24), cibenzone (25), diltiazem (26), nitrendipine (27), phenytoin (28), propranolol (29), risperidone (30) and verapamil (31)

EAD was induced by quinidine at its EFTPC<sub>max</sub>, by ajmaline at 10-fold its EFTPC<sub>max</sub> and by dofetilide at 30-fold its EFTPC<sub>max</sub> while no EAD was induced by amiodarone and tedisamil.

On the epimyocardial cells, the global picture (Fig. 6B) was somewhat similar except that EAD was now observed with quinidine (class I) at 3-fold its EFTPC<sub>max</sub>, with cisapride and terfenadine (class II) at 30-fold their EFTPC<sub>max</sub> while no EAD was observed with prenylamine (class II).

On the midmyocardial cells, EAD (Fig. 6C) was observed with cibenzoline (class V) and imipramine (class IV) only at 100-fold their EFTPC<sub>max</sub> or with propafenone (class IV) at 10-fold its EFTPC<sub>max</sub>. Within class III, EAD was observed with bepridil at 10-fold its EFTPC<sub>max</sub>, with haloperidol and sertindole at 30-fold their EFTPC<sub>max</sub>, and with pimoziide at 100-fold its EFTPC<sub>max</sub> while no EAD was observed with chlorpromazine. Within class II, all the various drugs induced EAD with a profile similar to that observed on endomyocardial cells. Within class I, amiodarone did not induce any EAD, while tedisamil induced EAD at 100-fold its EFTPC<sub>max</sub>, ajmaline and dofetilide at 30-fold their EFTPC<sub>max</sub> and quinidine at its EFTPC<sub>max</sub>.

## Discussion

### EAD formation

The importance of EAD formation in cardiac safety pharmacology is now fully recognized as EADs were identified as being primary to Tdp induction in many non-clinical pro-arrhythmia models [2, 11, 15, 16]. As a result, identification of all the components leading to EAD remains a major objective. The present study simulated various conditions of EAD formation using non-failing human ventricular myocytes (ORD model, [29]) and identified the role of ionic currents, bradycardia and cellular type in EAD formation.

Among the various cardiac currents,  $I_{Kr}$  was crucial [34 for review] because of its pivotal role in EAD formation as experimentally observed using dofetilide or E-4031 ( $I_{Kr}$  inhibitors) in various experimental models [26]. Our simulations using the ORD model confirmed the unique role of  $I_{Kr}$  inhibition in EAD formation as it was the only change that was able, by itself, to facilitate EAD formation. Our simulations showed an EAD at a take-off membrane voltage of  $-22$  mV, confirming take-off values observed in human isolated endomyocytes [10] or in human-induced pluripotent stem cell-derived cardiomyocytes [19]. Never-

theless, a multiple ion channel control had to be taken into account as our simulations showed that multiple other currents contributed to EAD formation or prevention under sub- or up-threshold EAD conditions. Under sub-threshold EAD conditions, only  $I_{Ks}$  inhibition facilitated EAD formation, which confirmed experimental results observed on rabbit isolated Langendorff-perfused hearts [9], open-chest anesthetized New Zealand white rabbit [21], rabbit ventricle [37] and human ventricle [13]. After their activation under sub-threshold EAD conditions, the seven currents facilitating EAD formation were ranked from least to most powerful as follows:  $I_{CaNa} \approx I_{Cab} < I_{Nab} < I_{NaL} \ll I_{NaCai} \approx I_{NaCass} < I_{CaL}$ . Such an effect of  $I_{CaL}$  activation was experimentally demonstrated with BAY K 8644 ( $Ca^{++}$  agonist) in canine isolated ventricular papillary muscles and Purkinje fibre for example [25, 31]. After their inhibition under up-threshold conditions of EAD, the five currents suppressing EAD were ranked from least to most powerful as follows:  $I_{NaL} < I_{Na} < I_{NaCai} \approx I_{NaCass} < I_{CaL}$ , confirming effects of RSD1235 ( $I_{NaL}$  blocker) on EAD induced by dofetilide on the rabbit isolated Purkinje fibres [30], mexiletine ( $I_{Na}$  blocker) in the dog isolated left ventricle [36], SEA-0400 ( $Na^+/Ca^{++}$  exchanger inhibitor) in canine isolated ventricular papillary muscles [25], KN-93 ( $Ca^{++}$ /calmodulin kinase inhibitor) and  $Ca^{++}$  antagonists in the rabbit isolated heart [1] or nicardipine ( $I_{CaL}$  blocker) in the rabbit isolated sinoatrial node cells [20]. After their activation under up-threshold conditions of EAD, the six currents suppressing EAD were ranked from least to most powerful as follows:  $I_{CaK} \ll I_{to} < I_{Kb} \ll I_{K1} < I_{Ks} \approx I_{NaK}$ . Such an effect of  $I_{Ks}$  activation has already been reported with L364,373 ( $I_{Ks}$  activator) in the guinea pig isolated cardiomyocytes [27]. In summary, our simulations confirmed in the human species the major role of  $I_{Kr}$ ,  $I_{Ks}$ ,  $I_{CaL}$  and  $I_{NaCa}$  in the EAD ionic mechanism as previously discussed [see 41 for review]: the interaction between deactivation of repolarizing currents (mainly  $I_{Kr}$  and to a lesser extent  $I_{Ks}$ ) together with  $I_{CaL}$  reactivation and  $I_{NaCa}$  synergistic increase in the adequate window voltage range (-30 to 0 mV) during AP repolarisation facilitated EAD formation.

At the cellular level, EAD formation was reported to be associated with various changes in ionic currents properties, resulting in APD prolongation and/or AP triangulation [16, 40, 41]. For example, Lu et al. [18] described a relationship between amplitude of APD prolongation and EAD incidence in rabbit isolated

Purkinje fibres. The present results showed that  $I_{CaL}$  activation induced longer APD prolongation and higher AP triangulation than  $I_{Kr}$  inhibition. Moreover, this APD prolongation was observed in a different voltage range with  $I_{CaL}$  activation or  $I_{Kr}$  inhibition. This observation confirmed in the human species that APD prolongation and/or the presence of AP triangulation were not the major parameters responsible for EAD induction and that the EAD voltage window was of importance, as already discussed by Weiss et al. [41].

The present simulations clearly confirmed the facilitating role of bradycardia on EAD formation as previously experimentally observed [40, 41]: a CL window of 3790–3800 ms was the threshold above or below the one at which an EAD was always or never observed with our simulations on the human endocardial cell under 85%  $I_{Kr}$  inhibition.

In addition to the role of ionic currents and bradycardia, EAD formation was also dependent on the cell type: midmyocardial cells were reported to be more susceptible to develop EAD than epi or endomyocardial cells leading to a transmural dispersion repolarisation and TdP as demonstrated with left ventricular wedge preparation for example [16, 40, 41]. This cell heterogeneity was confirmed by the present simulations. A higher susceptibility of midmyocardial cells to develop EAD was observed: 62%  $I_{Kr}$  inhibition was high enough to induce EAD in midmyocardial cells whereas 85 and 91%  $I_{Kr}$  inhibition were required for endo- and epimyocardial cells respectively, under a CL of 4000 ms.

### EAD and cardiac safety assessment

Our simulations clearly demonstrated the important role played by multiple ionic channels on both AP shape and EAD formation. By modelling the actions of drugs taking into account the ratio of their  $IC_{50}$  for  $I_{Kr}$ ,  $I_{Na}$  and  $I_{CaL}$  currents to  $EFTPC_{max}$ , Mirams et al. [23] showed that  $APD_{90}$  at low/medium/high  $EFTPC_{max}$  was a better predictive single marker for drug Tdp risk than the ratio  $IC_{50 I_{Kr}}/EFTPC_{max}$  previously used. Taking into account the same parameters in the ORd model, could our simulations of EAD formation add some value to early cardiac safety assessment? Despite some differences in sensitivity between endo-, epi- and midmyocardial cells, an excellent relationship between Tdp risk classification and EAD formation was observed with the ORd model, confirming most of the results from the rabbit isolated heart model [12, 14, 39], the dog isolated wedge preparation [7] and clinical data

[42]. Indeed, EAD was not observed with drugs from classes IV and V ('safe' classes), EAD was observed with some drugs from class III ('dangerous' class) and EAD was always induced with drugs from classes I and II ('prohibited' classes) ranked from 1 to 100-fold their  $EFTPC_{max}$ . Amiodarone from class I (false negative) or propafenone from class IV (false positive) were the only two exceptions observed with the results obtained from the most sensitive cell (the midmyocardial cell). We never observed EAD formation with amiodarone even at 100-fold its  $EFTPC_{max}$ , confirming Mirams' results [23] and experimental results already described on the dog isolated left ventricle [7], on the rabbit isolated heart [12] and on a rabbit model of acute atrioventricular block [22]. We observed EAD formation with propafenone on midmyocardial cells at 10-fold its  $EFTPC_{max}$  while no EAD at all was induced on epi- and endomyocardial cells even at 100-fold its  $EFTPC_{max}$ . More research is required in order to explain this single conflicting result as propafenone was observed as safe by Mirams' study [23] and did not affect repolarisation time in a clinical situation [35]. However, there is doubt that this study had some limitations: only 31 drugs and only three ionic currents out of 16 were taken into account. A full picture of activity on the various currents with a larger set of drugs would be required to study the drug ability to induce EAD formation and reinforce the confidence in the relationship between Tdp risk classification and EAD formation highlighted by the present study. The role of many ionic currents in EAD facilitation was identified in this study and, relative to this, the effects of drugs on  $I_{Ks}$  and  $I_{NaCa}$  will certainly be included in a future study. Other limitations may be the variations in the determination not only of  $EFTPC_{max}$  but also of  $IC_{50}$  (determined in the used data set [23] by the whole cell patch clamp technology on human cells for  $I_{Na}$  and  $I_{Kr}$  but on guinea pig for  $I_{CaL}$ ). Finally, mathematical algorithms such as the ORd algorithm still require refinement in order to better reflect the biological reality experimentally observed.

The present study was constructed based on the drug data set described by Mirams et al. [23]. We based the Tdp risk prediction on facilitation of EAD formation as simulated by the ORd model [29] while the study of Mirams et al. based their Tdp risk prediction on the maximum  $APD_{90}$  as simulated by the Grandi et al. model [8]. As discussed by O'Hara et al. [29], the ORd model offers closer correspondence to experimental measurements of various APDs and is the only algorithm able to reproduce EAD within the

human situation due to a better formulation of  $I_{CaL}$  inactivation compared to the model of Grandi et al. Moreover, our simulations showed that facilitation of EAD formation is sensitive not only to APD prolongation and/or AP triangulation but also to the membrane voltage range in which the major part of the APD prolongation lingers. Nevertheless, notwithstanding the limitations of both models and the differences between both models, our study was in agreement with the study of Mirams et al. [23], highlighting the major importance of multiple ionic currents and providing for cardiac early safety pharmacology an improved prediction of Tdp risk compared to methods based only on  $I_{Kr}$  block effect.

In conclusion, even and perhaps especially during the early process of compounds selection, an integrated picture of all involved cardiac currents activities should be taken into account when making cardiac safety pharmacology decisions. Due to the low throughput/expensive selection process based on isolated cell/tissue or animal experiments, *in silico* simulation early screening [24, 38] could be of a great help, since detection of EAD formation remains a good marker of potential cardiac liabilities (Tdp, polymorphic ventricular tachycardia or ventricular fibrillation). Moreover, this *in silico* simulation screening is faster, easier and less expensive than animal experiments and could be applied to a large number of drugs during the research process. These simulations could be carried out in a first screening step, where the compound affinities for various cardiac channels were already known, in order to determine a cardiac safety index, or in a second screening step in order to help understanding and/or extrapolation to the human situation of results already obtained in isolated cell/tissue or animal experiments. These *in silico* simulations could be used (i) to test different combinations of cardiac current inhibition and/or activation, (ii) to test the effect of various experimental conditions such as different heart rates or ionic composition or (iii) to compare results among various species and extrapolate these to the human situation. Nevertheless, these studies conducted at the cellular level remain an interesting but limited indication as tissue synchronisation and propagation of EAD across the whole heart are of major importance in order to understand the real picture of the *in vivo* situation. Such simulations are now in progress [41, 43] and will be of major help in the near future in order to reinforce cardiac safety pharmacology.

---

**Acknowledgment:**

The author wishes to thank Dr. O'Hara for his helpful suggestions and comments.

---

**References:**

1. Anderson ME, Braun AP, Wu Y, Lu T, Wu Y, Schulman H, Sung RJ: KN-93, an inhibitor of multifunctional  $Ca^{++}$ /calmodulin-dependent protein kinase, decreases early after-depolarisations in rabbit heart. *J Pharmacol Exp Ther*, 1998, 287, 996–1006.
2. Bass AS, Darpo B, Breidenbach A, Bruse K, Feldman HS, Garnes D, Hammond T et al.: International Life Sciences Institute (Health and Environmental Sciences Institute, HESI) initiative on moving towards better predictors of drug-induced torsades de pointes. *Br J Pharmacol*, 2008, 154, 1491–1501.
3. Cavero I: Exploratory safety pharmacology: a new safety paradigm to de-risk drug candidates prior to selection for regulatory science investigations. *Expert Opin Drug Saf*, 2009, 8, 627–647.
4. Chen X, Cordes JS, Bradley JA, Sun Z, Zhou J: Use of arterially perfused rabbit ventricular wedge in predicting arrhythmogenic potentials of drugs. *J Pharmacol Toxicol Methods*, 2006, 54, 261–272.
5. Clusin WT: Calcium and cardiac arrhythmias: DADs, EADs and alternans. *Crit Rev Clin Lab Sci*, 2003, 40, 337–375.
6. Davies MR, Mistry HB, Hussein L, Pollard CE, Valentin JP, Swinton J, Abi-Gerges N: An in silico canine cardiac midmyocardial action potential duration model as a tool for early drug safety assessment. *Am J Physiol Heart Circ Physiol*, 2012, 302, H1466–H1480.
7. Fenichel RR, Malik M, Antzelevitch C, Sanguinetti M, Roden DM, Priori SG, Ruskin JN et al.: Drug-induced torsades de pointes and implications for drug development. *J Cardiovasc Electrophysiol*, 2004, 15, 475–495.
8. Grandi E, Pasqualini FS, Bers DM: A novel computational model of the human ventricular action potential and Ca transient. *J Mol Cell Cardiol*, 2010, 48, 112–121.
9. Guérard NC, Traebert M, Suter W, Dumotier BM: Selective block of IKs plays a significant role in MAP triangulation induced by IKr block in isolated rabbit heart. *J Pharmacol Toxicol Methods*, 2008, 58, 32–40.
10. Guo D, Liu Q, Liu T, Elliott G, Gingras M, Kowey PR, Yan GX: Electrophysiological properties of HBI-3000: a new antiarrhythmic agent with multiple-channel blocking properties in human ventricular myocytes. *J Cardiovasc Pharmacol*, 2011, 57, 79–85.
11. Hondeghem LM, Dumotier B, Traebert M: Oscillations of cardiac wave length and proarrhythmia. *Naunyn Schmiedeberg's Arch Pharmacol*, 2010, 382, 367–376.
12. Hondeghem LM, Lu HR, van Rossem K, De Clerck F: Detection of proarrhythmia in the female rabbit heart: blinded validation. *J Cardiovasc Electrophysiol*, 2003, 14, 287–294.
13. Jost N, Papp JG, Varró A: Slow delayed rectifier potassium current (IKs) and the repolarization reserve. *Ann Noninvasive Electrocardiol*, 2007, 12, 64–78.
14. Lawrence CL, Bridgland-Taylor MH, Pollard CE, Hammond TG, Valentin JP: A rabbit Langendorff heart proarrhythmia model: predictive value for clinical identification of torsades de pointes. *Br J Pharmacol*, 2006, 149, 845–860.
15. Lawrence CL, Pollard CE, Hammond TG, Valentin JP: In vitro models of proarrhythmia. *Br J Pharmacol*, 2008, 154, 1516–1522.
16. Lawrence CL, Pollard CE, Hammond TG, Valentin JP: Nonclinical proarrhythmia models: predicting torsades de pointes. *J Pharmacol Toxicol Methods*, 2005, 52, 46–59.
17. Lu HR, Vlamincx E, Teisman A, Gallacher DJ: Choice of cardiac tissue plays an important role in the evaluation of drug-induced prolongation of the QT interval in vitro in rabbit. *J Pharmacol Toxicol Methods*, 2005, 52, 90–105.
18. Lu HR, Vlamincx E, Van Ammel K, De Clerck F: Drug-induced long QT in isolated rabbit Purkinje fibers: importance of action potential duration, triangulation and early after-depolarisations. *Eur J Pharmacol*, 2002, 452, 183–192.
19. Ma J, Guo L, Fiene SJ, Anson BD, Thomson JA, Kamp TJ, Kolaja KL et al.: High purity human-induced pluripotent stem cell-derived cardiomyocytes: electrophysiological properties of action potentials and ionic currents. *Am J Physiol Heart Circ Physiol*, 2011, 301, H2006–H2017.
20. Matsuda T, Kurata Y: Effects of nicardipine and bupivacaine on early after-depolarisation in rabbit sinoatrial node cells: a possible mechanism of bupivacaine-induced arrhythmias. *Gen Pharmacol*, 1999, 33, 115–125.
21. Michael G, Dempster J, Kane KA, Coker SJ: Potentiation of E-4031-induced torsade de pointes by HMR1556 or ATX-II is not predicted by action potential short-term variability or triangulation. *Br J Pharmacol*, 2007, 152, 1215–1227.
22. Milberg P, Ramtin S, Mönning G, Osada N, Wasmer K, Breithardt G, Haverkamp W, Eckardt L: Comparison of the in vitro electrophysiologic and proarrhythmic effects of amiodarone and sotalol in a rabbit model of acute atrioventricular block. *J Cardiovasc Pharmacol*, 2004, 44, 278–286.
23. Mirams GR, Cui Y, Sher A, Fink M, Cooper J, Heath BM, McMahon NC et al.: Simulation of multiple ion channel block provides improved early prediction of compounds' clinical torsadogenic risk. *Cardiovasc Res*, 2011, 91, 53–61.
24. Mirams GR, Noble D: Is it time for in silico simulation of drug cardiac side effects? *Ann NY Acad Sci*, 2011, 1245, 44–47.
25. Nagy ZA, Virág L, Tóth A, Biliczki P, Acsai K, Bányász T, Nánási P et al.: Selective inhibition of sodium-calcium exchanger by SEA-0400 decreases early and delayed after-depolarisation in canine heart. *Br J Pharmacol*, 2004, 143, 827–831.
26. Nalos L, Varkevisser R, Jonsson MK, Houtman MJ, Beekman JD, van der Nagel R, Thomsen MB et al.: Comparison of the IKr blockers moxifloxacin, dofetilide and E-4031 in five screening models of pro-arrhythmia

- reveals lack of specificity of isolated cardiomyocytes. *Br J Pharmacol*, 2012, 165, 467–478.
27. Nissen JD, Diness JG, Diness TG, Hansen RS, Grunnet M, Jespersen T: Pharmacologically induced long QT type 2 can be rescued by activation of  $I_{Ks}$  with benzodiazepine R-L3 in isolated guinea pig cardiomyocytes. *J Cardiovasc Pharmacol*, 2009, 54, 169–177.
  28. O'Hara T, Rudy Y: Quantitative comparison of cardiac ventricular myocyte electrophysiology and response to drugs in human and non-human species. *Am J Physiol Heart Circ Physiol*, 2012, 302, H1023–H1030.
  29. O'Hara T, Virág L, Varró A, Rudy Y: Simulation of the undiseased human cardiac ventricular action potential: model formulation and experimental validation. *PLoS Comput Biol*, 2011, 7, e1002061.
  30. Orth PM, Hesketh JC, Mak CK, Yang Y, Lin S, Beach GN, Ezrin AM, Fedida D: RSD1235 blocks late  $I_{Na}$  and suppresses early after-depolarisations and *torsades de pointes* induced by class III agents. *Cardiovasc Res*, 2006, 70, 486–496.
  31. Patterson E, Scherlag BJ, Lazzara R: Early after-depolarisations produced by d,l-sotalol and clofilium. *J Cardiovasc Electrophysiol*, 1997, 8, 667–678.
  32. Polak S, Wiśniowska B, Glinka A, Polak M: Tox-Database.net: a curated resource for data describing chemical triggered in vitro cardiac ion channels inhibition. *BMC Pharmacol Toxicol*, 2012, 13, 6
  33. Pugsley MK, Authier S, Curtis MJ: Principles of safety pharmacology. *Br J Pharmacol*, 2008, 154, 1382–1399.
  34. Redfern WS, Carlsson L, Davis AS, Lynch WG, MacKenzie I, Palethorpe S, Siegl PK et al.: Relationships between preclinical cardiac electrophysiology, clinical QT interval prolongation and torsade de pointes for a broad range of drugs: evidence for a provisional safety margin in drug development. *Cardiovasc Res*, 2003, 58, 32–45.
  35. Sarubbi B, Ducceschi V, Briglia N, Mayer MS, Santangelo L, Iacono A: Compared effects of sotalol, flecainide and propafenone on ventricular repolarization in patients free of underlying structural heart disease. *Int J Cardiol*, 1998, 66, 157–164.
  36. Sicouri S, Antzelevitch D, Heilmann C, Antzelevitch C: Effects of sodium channel block with mexiletine to reverse action potential prolongation in *in vitro* models of the long term QT syndrome. *J Cardiovasc Electrophysiol*, 1997, 8, 1280–1290.
  37. So PP, Hu XD, Backx PH, Puglisi JL, Dorian P: Blockade of  $I_{Ks}$  by HMR 1556 increases the reverse rate-dependence of refractoriness prolongation by dofetilide in isolated rabbit ventricles. *Br J Pharmacol*, 2006, 148, 255–263.
  38. Soubret A, Helmlinger G, Dumotier B, Bibas R, Georgieva A: Modeling and simulation of preclinical cardiac safety: towards an integrative framework. *Drug Metab Pharmacokinet*, 2009, 24, 76–90.
  39. Steidl-Nichols JV, Hanton G, Leaney J, Liu RC, Leishman D, McHarg A, Wallis R: Impact of study design on proarrhythmia prediction in the SCREENIT rabbit isolated heart model. *J Pharmacol Toxicol Methods*, 2008, 57, 9–22.
  40. Volders PGA, Vos MA, Szabo B, Sipido KR, de Groot MSH, Gorgels APM, Wellens HJJ, Lazzara R: Progress in the understanding of cardiac early after-depolarizations and torsades de pointes: time to revise current concepts. *Cardiovasc Res*, 2000, 46, 376–392.
  41. Weiss JN, Garfinkel A, Karagueuzian HS, Chen PS, Qu Z: Early after-depolarizations and cardiac arrhythmias. *Heart Rhythm*, 2010, 7, 1891–1899.
  42. Yap YG, Camm AJ: Drug induced QT prolongation and torsades de pointes. *Heart*, 2003, 89, 1363–1372.
  43. Zemzemi N, Bernabeu MO, Saiz J, Cooper J, Pathmanathan P, Mirams GR, Pitt-Francis J, Rodriguez B: Computational assessment of drug-induced effects on the electrocardiogram: from ion channel to body surface potentials. *Br J Pharmacol*, 2013, 168, 718–733.

**Received:** September 6, 2012; **in the revised form:** May 13, 2013; **accepted:** May 16, 2013.